MJFAS
Malaysian Journal of Fundamental and Applied Sciences

Sohut *et al.* | Malaysian Journal of Fundamental and Applied Sciences, Vol. 20 (2024) 360-377

RESEARCH ARTICLE

Hybrid Nanofluids Flow over a Vertical Cylinder with Heat Source/Sink and Prescribed Surface Heat Flux

Farizza Haniem Sohut[a]*, Siti Khuzaimah Soid[b], Anuar Ishak[a]

[a]Department of Mathematical Sciences, Universiti Kebangsaan Malaysia, 43600 Bangi, Selangor, Malaysia; [b]College of Computing, Informatics and Mathematics Universiti Teknologi MARA, 40450 Shah Alam, Selangor, Malaysia

Abstract This work presents the steady mixed convection in Al_2O_3-Cu/water hybrid nanofluids along a vertically stretching/shrinking cylinder with the prescribed surface heat flux and the effects of heat source/sink. The governing hybrid nanofluids model was simplified using a similarity transformation. The bvp4c solver in MATLAB software is used to solve the hybrid nanofluids flow problem numerically. It is observed that two outcomes are feasible for the assisting and opposing flow regions $(\pm\lambda)$ as well as stretching and shrinking cases $(\pm\varepsilon)$. Besides that, the effects of the dimensionless parameters are analyzed graphically and tabularly. In particular, the critical point is reduced by 3% when the curvature parameter goes from 0 to 0.1 and from 0.1 to 0.2 when the cylinder is stretched. This means that the higher curvature parameter could delay the process of separating the boundary layer. It is noted that the positive heat source will decrease the fluid motions and reduce the shear stress on the surface. Moreover, Al_2O_3-Cu/water hybrid nanofluids have better performance in heat transfer and velocity of fluid flow than Al_2O_3/water nanofluids.

Keywords: Heat Source/Sink, Stretching Cylinder, Hybrid Nanofluids, Heat Flux, Dual Solutions, Stability Analysis.

Introduction

A flow of stagnation-point can be described as a point in the flow with an absence of fluid velocity located at the surface of an object, which causes the fluid to come to a halt in the stagnation region. When there is no fluid motion, the static pressure is greatest near the stagnation point. The study of stagnation-point flow is an important topic in fluid mechanics, and it has attracted the interest of many researchers because of its applications in industry and engineering fields such as flows over the tips of aircraft wings and submarines, designing cooling systems, accelerators, and others. The pioneering work in this area was done by Hiemenz in 1911, who discussed the two-dimensional (2-D) flow of a fluid near a stagnation point and developed an exact solution to the governing Navier-Stokes equations. Many authors have extended their work to different model problems. For example, Mahapatra and Gupta [2] explored the steady 2-D stagnation-point flow over a stretching sheet. Later, Ishak *et al*. [3] continued the research by adding mixed convection using a finite-different method. They discovered that the opposing flow had two solutions, while the aiding flow region only had a single solution. Meanwhile, Wang [4] considered both 2-D and axisymmetric stagnation flow over a shrinking sheet. In his research, he explored the effect of non-alignment for the first time and found that the flow structure is complicated. A year later, Ishak [5] extended the study of the flow with the prescribed wall heat flux. The study of the prescribed wall heat flux plays an important role in many industrial applications, such as thermal management of electronic devices, metal heat treatment, spray cooling, etc. [6]. Ishak [5] also diversifies this research for the different cases and effects of parameters [7–9]. Besides that, Awaludin *et al*. [10] investigated a similar problem as Ishak [5] with a horizontal cylinder and the effects of suction and injection. They discovered that the reduced curvature parameter affects boundary layer separation and that dual solutions exist for a certain range of curvature parameters. The problems related to the prescribed surface heat flux can also be found in references [11–15].

Physically, nanofluids are generated by distributing the solid particles into a base liquid, which has low thermal conductivity. For example, water, oils, and ethylene glycol. This is an innovative way to suspend

***For correspondence:**
p106827@siswa.ukm.edu.my

Received: 28 Oct. 2023
Accepted: 10 Jan. 2024

small solid particles in the fluid, such as metallic, non-metallic, and polymeric particles, to be mixed into the fluid. Nanofluids have become an interesting research topic for the past few years in convection heat transfer and can be found in the references [16–21]. According to Khan *et al*. [22], nanofluids are composed of nano-sized particles such as diamond and gold, as well as conventional base fluid. The thermal conductivity of conventional heat transfer is known to be poor and has been recognized experimentally. Therefore, many studies have been conducted to improve the mentioned issue. However, hybrid nanofluids are introduced to replace nanofluids. One of the reasons is that hybrid nanofluids have a wider absorption range, high thermal conductivity, low pressure drops, low friction loss, and so on compared to nanofluids. According to Suresh *et al*. [23], scholars have used various kinds of nanoparticles in their studies, including carbon nanotubes, metallic particles, and non-metallic particles. The thermal conductivity can be significantly improved if the nanoparticle materials, including metal (i.e., Al_2O_3/Ni, MgO/Fe, Al_2O_3/Cu), ceramics (i.e., SiO_2/Al_2O_3, Al_2O_3/TiO_2, CNT/Fe_3O_4) and polymer (i.e., Polymer/carbon nanotubes (CNT)) nanomaterials are properly selected. In addition, Suresh *et al*. [24] explored the effects of Al_2O_3-Cu/H_2O hybrid nanofluids on heat transfer and pressure drop features. The result shows that 0.1% Al_2O_3-Cu/H_2O hybrid nanofluids have a slightly higher friction factor compared to Al_2O_3/H_2O nanofluids, and it proves that hybrid nanofluids perform better than nanofluids. Furthermore, an investigation of natural convection in a sinusoidal corrugation of Al_2O_3-Cu/H_2O hybrid nanofluids in volume concentration (0 to 2%) is done by Takabi and Salehi [25]. From the analysis, hybrid nanofluids improve the heat transfer rate (perform better cooling and lower the temperature of the heated surface) compared to other fluids. The validation of the modeling and experimental data with Suresh *et al*. (2011) for a volume concentration of 2% with their new mathematical correlations of hybrid nanofluids exhibits a good agreement. Moreover, hybrid nanofluids are visibly effective in increasing thermal conductivity performance and have been proven by several researchers [26–31].

Recently, several studies have been conducted involving hybrid nanofluids. For example, Jamaludin *et al*. [32] analyzed the magnetohydrodynamics of Cu-Al_2O_3/H_2O hybrid nanofluids over a permeable stretching/shrinking sheet in the presence of a heat source or sink. The presence of the heat source or sink is also important in industrial processes such as cooling electronic devices. In addition, the quality of the final product depends on the heat control factor. According to Jamaludin *et al*. [32] after considering several aspects, few studies have been carried out to evaluate the influence of heat sources or sinks on the flow and heat transfer in nanofluids. In particular, Gorla *et al*. [33] focused on the heat source or sink effects on hybrid nanofluids flow in a square cavity. Then, Armaghani *et al*. [34] investigated similar cases as the above-mentioned authors in an L-shaped cavity, and exploring the effect of its length on heat transfer performance was also one of their objectives. The outcomes show that using the greatest amount of sink power results in the best heat transfer performance. Other research on the effects of heat source or sink on hybrid nanofluids flow can also be found in Yaseen *et al*. [35] and Farooq *et al*. [36].

There are few studies done about mixed convection hybrid nanofluids flow with heat source or sink. Hence, the present work intends to explore the effects of the mixed convection Al_2O_3-Cu/H_2O hybrid nanofluids flow towards the vertical stretching/cylinder in the presence of the heat source/sink and the prescribed surface heat flux. By using the bvp4c solver in MATLAB software, the reduced ODEs are numerically solved. This hybrid nanofluids model is extended from Ishak [5], Waini *et al*. [15], and Sadighi *et al*. [37]. The numerical findings obtained are shown in tables and figures, and they have been validated by previous research. Besides that, the novelty of the study is attained by the finding of two solutions at the stretching and shrinking surfaces and in both aiding and opposing fluid flow. Also, stability inquiry is performed to prove the physical outcome in the long run.

Problem Formulation

A steady, two-dimensional, laminar, and hybrid nanofluids flow of incompressible mixed convection along a vertically stretching or shrinking cylinder of radius R at an ambient temperature T_∞ is considered, as illustrated in Figure 1. The surface is assumed to be impermeable and the cylinder is being stretched/shrunk in the axial direction with the linear velocity $U_w(x) = b(x/l)$ subjected to the prescribed heat flux, $q_w(x) = T_0(x/l)$ with constant b and reference temperature, T_0. Besides, the velocity of the freely flowing stream is $u_e(x) = a_e(x/l)$, where l is the cylinder's characteristic length, and a_e is a positive constant. Here, u and v are velocity components along the x and r directions, while x and r are coordinates measured in the radial and axial direction of the cylinder, respectively, and g is the acceleration due to gravity.

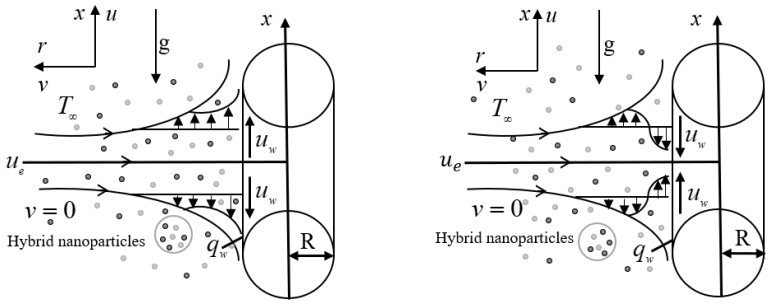

Figure 1. Physical configuration. (a) Stretching cylinder. (b) Shrinking cylinder

The flow equations for the hybrid nanofluids model following (see [5,15,37]).

$$\frac{\partial(ur)}{\partial x}+\frac{\partial(vr)}{\partial r}=0 \tag{1}$$

$$u\frac{\partial u}{\partial x}+v\frac{\partial u}{\partial r}-u_e\frac{\partial u_e}{\partial x}=\frac{\mu_{hf}}{\rho_{hf}}\frac{1}{r}\frac{\partial}{\partial r}\left(r\frac{\partial u}{\partial r}\right)+\frac{(\rho\beta)_{hf}}{\rho_{hf}}(T-T_\infty)g \tag{2}$$

$$(\rho C_p)_{hf}\left(u\frac{\partial T}{\partial x}+v\frac{\partial T}{\partial r}\right)=k_{hf}\frac{1}{r}\frac{\partial}{\partial r}\left(r\frac{\partial T}{\partial r}\right)+Q_0(T-T_\infty) \tag{3}$$

while the boundary conditions are

$$\begin{aligned} &r=R(x): && u=U_w(x), && v=0, && -k_{hf}\frac{\partial T}{\partial r}=q_w(x),\\ &r\to\infty: && u\to u_e(x)=a_e(x/l), && && T\to T_\infty\ . \end{aligned} \tag{4}$$

u and v are the velocity components along x and r directions, T is the temperature of the fluid, q_w is the prescribed wall heat flux, Q_0 is the dimensionless heat generation/absorption coefficient, and $a_e>0$ is a positive constant, respectively. Additionally, μ is the dynamic viscosity, ρ is the density, k is the thermal conductivity, $(\rho\beta)$ represents the thermal expansion coefficient and (ρC_p) is the specific heat capacity. Note that, $\varphi_{hf}=\varphi_1+\varphi_2$ is the hybrid nanoparticles volume fraction, where φ_1 and φ_2 are alumina (Al_2O_3) and copper (Cu) nanoparticles volume fraction. Furthermore, the subscripts *n1* and *n2* indicate the nanoparticles Al_2O_3 and Cu, while *hf* and *f* stand for the hybrid nanofluids and base fluid, respectively. In this study, the Al_2O_3-Cu/H_2O hybrid nanofluids are considered because both alumina and copper nanoparticles individually have high thermal conductivity. The combination of these two nanoparticles can synergistically enhance the overall thermal conductivity of the nanofluids. Besides that, the enhanced thermal conductivity of the hybrid nanofluids contributes to improved heat transfer efficiency.

Table 1 provides the properties of the nanoparticles (Al_2O_3 and Cu) and water, following Oztop and Abu-Nada [38], Waini *et al*. [39], and Khashi'ie *et al*. [40] for the references. In addition, the thermophysical correlations of hybrid nanofluids following Takabi and Salehi [25] are shown in Table 2.

Table 1. Thermophysical properties

Physical Properties	Al_2O_3	Cu	Water
Prandtl number, Pr			6.2
$k\,(W/mK)$	40	400	0.613
$C_p\,(J/KgK)$	765	385	4179
$\rho\,(kg/m^3)$	3970	8933	997.1
$\beta\times10^{-5}\,(1/K)$	0.85	1.67	21

Table 2. Thermophysical properties of Al_2O_3 – Cu/H_2O

Properties	Hybrid Nanofluids
Density, ρ	$\rho_{hf} = \varphi_1\rho_{n1} + \varphi_2\rho_{n2} + (1-\varphi_{hf})\rho_f$
Dynamic viscosity, μ	$\mu_{hf} = \mu_f (1-\varphi_1-\varphi_2)^{-2.5}$
Thermal conductivity, k	$\frac{k_{hf}}{k_f} = \left\{\frac{\varphi_1 k_{n1}+\varphi_2 k_{n2}}{\varphi_1+\varphi_2} + 2k_f + 2(\varphi_1 k_{n1}+\varphi_2 k_{n2}) - 2(\varphi_1+\varphi_2)k_f\right\}\times \left\{\frac{\varphi_1 k_{n1}+\varphi_2 k_{n2}}{\varphi_1+\varphi_2} + 2k_f - (\varphi_1 k_{n1}+\varphi_2 k_{n2}) + (\varphi_1+\varphi_2)k_f\right\}^{-1}$
Heat capacity, (ρC_p)	$(\rho C_p)_{hf} = \varphi_1(\rho C_p)_{n1} + \varphi_2(\rho C_p)_{n2} + (1-\varphi_{hf})(\rho C_p)_f$
Thermal expansion, $(\rho\beta)$	$(\rho\beta)_{hf} = \varphi_1(\rho\beta)_{n1} + \varphi_2(\rho\beta)_{n2} + (1-\varphi_{hf})(\rho\beta)_f$

To get similarity solutions, we adopt the transformation variables following (Ishak [5];Waini *et al*. [15]):

$$\psi = (u_e \nu_f x)^{1/2} R f(\eta), \qquad \eta = \frac{r^2-R^2}{2R}\sqrt{\frac{u_e}{\nu_f x}}, \qquad T = T_\infty + \frac{q_w}{k_f}\sqrt{\frac{\nu_f l}{a_e}}\theta(\eta) \tag{5}$$

where prime denotes differentiation w.r.t. to η, f and θ are the dimensionless stream function and temperature, and η is the similarity variable, respectively. Besides, ψ is the stream function defined as $u = r^{-1}(\partial\psi/\partial r)$ and $v = -r^{-1}(\partial\psi/\partial x)$, which identically satisfies Equation (1) and ν_f is the fluid kinematic viscosity.

The similarity variables (6) are substituted into equations (2) to (4). The transformed ODEs are as follows:

$$\frac{\mu_{hf}}{\mu_f}\left[(2\eta K+1)f'''(\eta)+2Kf''(\eta)\right] + \frac{(\rho\beta)_{hf}}{(\rho\beta)_f}\lambda\theta(\eta) - \frac{\rho_{hf}}{\rho_f}\left(-1+f'^2(\eta)-f(\eta)f''(\eta)\right) = 0 \tag{6}$$

$$\frac{k_{hf}}{\mathrm{Pr}\,k_f}\left[(1+2\eta K)\theta''(\eta)+2K\theta'(\eta)\right] + \delta\theta(\eta) + \frac{(\rho C_p)_{hf}}{(\rho C_p)_f}\left(-f'(\eta)\theta(\eta)+f(\eta)\theta'(\eta)\right) = 0 \tag{7}$$

subject to

$$\begin{aligned} &f(0)=0, \quad f'(0)=\varepsilon, \quad \text{and} \quad \theta'(0) = -\frac{1}{k_{hf}/k_f}, \quad \text{at} \quad \eta = 0 \\ &f'(\eta)\to 1, \quad \theta(\eta)\to 0, \quad \text{as} \quad \eta\to\infty \end{aligned} \tag{8}$$

where λ, K, Pr, δ, and ε are the constant mixed convection, curvature, Prandtl number, constant heat source/sink, and constant stretching/shrinking parameters, respectively. Besides that, Gr_x is the Grashof number due to temperature and Re_x is the Reynolds number.

$$\begin{aligned} &\mathrm{Pr} = \frac{\nu_f}{\alpha_f}, \quad K = \frac{1}{R}\sqrt{\frac{\nu_f l}{a_e}}, \quad \lambda = \frac{Gr_x}{\mathrm{Re}_x^{\,2}}(=\text{const.}), \quad \mathrm{Re}_x = \frac{u_e x}{\nu_f}, \\ &Gr_x = \frac{g\beta_f(T_w-T_\infty)x^3}{\nu_f^{\,2}}, \quad \delta = \frac{lQ_0}{a_e(\rho C_p)_f}(=\text{const.}), \quad \varepsilon = \frac{b}{a_e} \end{aligned} \tag{9}$$

where $\lambda<0$ represents the assisting flow and $\lambda>0$ represents the aiding flow, respectively. Meanwhile, $\delta>0$, and $\delta<0$ imply the heat source and heat sink, correspondingly. It is noteworthy to mention that $\varepsilon>0$ and $\varepsilon<0$ are referred to the stretching and shrinking cylinder.

The local skin friction coefficient and local Nusselt number are given by:

$$C_f = \frac{\mu_{hf}}{\rho_f u_e^{\,2}(x)}\left(\frac{\partial u}{\partial r}\right)_{r=R}, \qquad Nu_x = -\frac{xk_{hf}}{k_f(T_w-T_\infty)}\left(\frac{\partial T}{\partial r}\right)_{r=R} \tag{10}$$

Substitute (5) into (10), we get

$$\sqrt{\mathrm{Re}_x}C_f = \frac{\mu_{hf}}{\mu_f} f''(0), \qquad \frac{1}{\sqrt{\mathrm{Re}_x}} Nu_x = \frac{1}{\theta(0)} \tag{11}$$

Analysis of Temporal Stability

Stability analysis is a general term applied to various systems and disciplines. Meanwhile, temporal stability analysis specifically emphasizes the temporal aspect of stability, considering how a system's behavior changes over time. The temporal stability inquiry is needed to determine the reliability of the non-unique similarity solutions. The existence of non-unique solutions to Equations (7) to (10) is observed for a given set of physical parameters. Merkin [41] initiated this stability analysis method in 1986 and Weidman *et al*. [42] introduced a dimensionless time variable, τ to explore the long-term stability of the solutions. From the evaluation, they concluded that the first solution is stable, while the second solution is not. For this analysis, an unsteady problem is considered. The new Equations (2)-(4) are given as follows:

$$\rho_{hf}\left(\frac{\partial u}{\partial t} + u\frac{\partial u}{\partial x} + v\frac{\partial u}{\partial r} - u_e\frac{\partial u_e}{\partial x}\right) = \frac{\mu_{hf}}{r}\frac{\partial}{\partial r}\left(r\frac{\partial u}{\partial r}\right) + (\rho\beta)_{hf}(T - T_\infty)g \tag{12}$$

$$(\rho C_p)_{hf}\left(\frac{\partial T}{\partial t} + u\frac{\partial T}{\partial x} + v\frac{\partial T}{\partial r}\right) = \frac{k_{hf}}{r}\frac{\partial}{\partial r}\left(r\frac{\partial T}{\partial r}\right) + Q_0(T - T_\infty) \tag{13}$$

The new variables based on Equation (6) following Waini *et al*. [15]

$$\psi = (u_e v_f x)^{1/2} Rf(\eta,\tau), \quad \eta = \frac{r^2 - R^2}{2R}\sqrt{\frac{u_e}{v_f x}}, \quad T = T_\infty + \frac{q_w}{k_f}\sqrt{\frac{v_f l}{a_e}}\theta(\eta,\tau), \quad \tau = \left(\frac{a_e}{l}\right)t \tag{14}$$

Using (14), Equations (12) and (13) can be rewritten as

$$\frac{\mu_{hf}}{\mu_f}\left[(2\eta K + 1)\frac{\partial^3 f}{\partial \eta^3} + 2K\frac{\partial^2 f}{\partial \eta^2}\right] + \frac{(\rho\beta)_{hf}}{(\rho\beta)_f}\lambda\theta - \frac{\rho_{hf}}{\rho_f}\left(-1 + \left(\frac{\partial f}{\partial \eta}\right)^2 - f\frac{\partial^2 f}{\partial \eta^2} + \frac{\partial^2 f}{\partial \eta\,\partial \tau}\right) = 0 \tag{15}$$

$$\frac{k_{hf}}{\mathrm{Pr}\,k_f}\left[(2\eta K + 1)\frac{\partial^2 \theta}{\partial \eta^2} + 2K\frac{\partial \theta}{\partial \eta}\right] + \delta\theta - \frac{(\rho C_p)_{hf}}{(\rho C_p)_f}\left(-f\frac{\partial \theta}{\partial \eta} + \theta\frac{\partial f}{\partial \eta} + \frac{\partial \theta}{\partial \tau}\right) = 0 \tag{16}$$

The conditions are

$$\begin{aligned} &f(0,\tau) = 0, \quad \frac{\partial f}{\partial \eta}(0,\tau) = \varepsilon, \quad \text{and} \quad \frac{\partial \theta}{\partial \eta}(0,\tau) = \frac{-1}{k_{hf}/k_f}, \quad \text{at} \quad \eta = 0 \\ &\frac{\partial f}{\partial \eta}(\eta,\tau) \to 1, \quad \theta(\eta,\tau) \to 0, \quad \text{as} \quad \eta \to \infty \end{aligned} \tag{17}$$

Equation (18) is then substituted into Equations (15) to (17) to examine the stability behavior of the solution obtained. The perturbation function is taken exponentially because these functions show the rapid growth or decline of the disturbance. These perturbation equations are introduced following Weidman *et al*. [42].

$$f(\eta,\tau) = f_0(\eta) + e^{-\gamma\tau}F_1(\eta) \text{ and } \theta(\eta,\tau) = \theta_0(\eta) + e^{-\gamma\tau}G_1(\eta) \tag{18}$$

Here, γ refers to an unknown eigenvalue parameter that determines the stability of the solutions whereas $f(\eta) = f_0(\eta)$ and $\theta(\eta) = \theta_0(\eta)$ are the steady solutions and $F_1(\eta)$ and $G_1(\eta)$ are a small relative to $f_0(\eta)$ and $\theta_0(\eta)$, respectively. By employing Equation (18), Equations (15) to (17) become

$$\begin{aligned} \frac{\mu_{hf}/\mu_f}{\rho_{hf}/\rho_f}\left[(2\eta K + 1)F_1''(\eta) + 2KF_1''(\eta)\right] + f_0''(\eta)F_1(\eta) + f_0(\eta)F_1''(\eta) - 2f_0'(\eta)F_1'(\eta) \\ + \frac{(\rho\beta)_{hf}/(\rho\beta)_f}{\rho_{hf}/\rho_f}\lambda G_1(\eta) + \gamma F_1'(\eta) = 0 \end{aligned} \tag{19}$$

$$\frac{k_{hf}}{\Pr k_f}\left[(2\eta K+1)G''(\eta)+2KG'(\eta)\right]+\delta G(\eta) + \frac{(\rho C_p)_{hf}}{(\rho C_p)_f}\left(\theta_0'(\eta)F(\eta)+f_0(\eta)G'(\eta)-f_0'(\eta)G(\eta)-\theta_0(\eta)F'(\eta)+\gamma G_0(\eta)\right)=0 \tag{20}$$

subject to

$$F_1(0)=0, \quad F_1'(0)=0, \quad G_1'(0)=0, \quad F_1'(\infty)\to 0, \quad G_1(\infty)\to 0, \tag{21}$$

For the present problem, we relaxed the derivative $F'(\eta)\to 0,$ as $\eta\to\infty$ in Equation (21) and replaced with the new boundary condition, which is $F_1''(0)=1$ following Harris *et al*. [43].

Results and Discussion

In order to obtain the numerical computation, Equations (6) and (7) with respect to Equation (8) are solved using the boundary value problem solver, bvp4c, in MATLAB software. The present study considers several parameters, such as the curvature parameter *K*, mixed convection parameter λ, the Cu nanoparticle volume fraction φ_2, the stretching/shrinking parameter ε, and the heat source/suction parameter δ in order to investigate the flow behavior and to determine all potential dual solutions in the opposing and assisting flow as well as stretching and shrinking surfaces. Further, to perform the stability analysis for the availability of dual solutions.

Moreover, Al_2O_3 nanoparticle volume fraction $\varphi_1=0.01$ and Prandtl number Pr = 6.2 are fixed throughout the numerical computation. Meanwhile, other parameters are varied such that $\lambda_c\le\lambda\le 10$, $0\le K\le 0.2$, $0\le\varphi_2\le 0.01$, and $-0.1\le\delta\le 0.1$. The parameter values are chosen based on the main reference, Waini *et al*. [15], and other references, Jamaludin *et al*. [32]. Subscripts 1 and 2, which correspond to alumina and copper, respectively, were used for clarity. Table 3 provides the comparison values of $f''(0)$ and $1/\theta(0)$ for different Pr values when *K* = 0 (flat plate) and $\lambda=1$ with the absence of δ, ε and φ_{hf} which show a favorable agreement with those obtained by Ishak [5] and Yacob and Ishak [13]. The results are compared for the first solution case only, with a different method used such as Keller-box, Runge-Kutta Fehlberg (RKF) and bvp4c methods.

Besides that, a comparison values of $f''(0)$ and $1/\theta(0)$ for several ε with the previously published literature by Waini *et al*. [15] using the bvp4c method is shown in Table 4. Those comparisons are found to be in favorable agreement. In addition, Table 5 demonstrates the numerical values of $\mathrm{Re}_x^{1/2}C_f$ and $\mathrm{Re}_x^{-1/2}Nu_x$ for the hybrid nanofluids when $\varphi_1=0.01$ and Pr = 6.2. From the observations, higher values of φ_2, *K* and λ will increase the values of $\mathrm{Re}_x^{1/2}C_f$ and $\mathrm{Re}_x^{-1/2}Nu_x$, respectively. An increase in the value of δ will result in an increment in $\mathrm{Re}_x^{1/2}C_f$ and a decrease in $\mathrm{Re}_x^{-1/2}Nu_x$. However, the values of $\mathrm{Re}_x^{1/2}C_f$ decrease, whereas the values of $\mathrm{Re}_x^{-1/2}Nu_x$ rise with the increase of ε (from shrinking to stretching).

Table 3. Validation of $f''(0)$, $1/\theta(0)$ for some Pr values when $\lambda=1$ and $\varphi_{hnf}=\varepsilon=\delta=0$

Pr	Ishak [5] (Keller-box)		Yacob and Ishak [13] (Keller-box & RKF)		Present (bvp4c)	
	$f''(0)$	$1/\theta(0)$	$f''(0)$	$1/\theta(0)$	$f''(0)$	$1/\theta(0)$
0.1			2.7301	0.3915	2.73006084	0.39150269
0.2			2.3307	0.5028	2.33070450	0.50278815
0.7	1.8339	0.7776	1.8339	0.7776	1.83387614	0.77760891
1.0	1.7338	0.8780	1.7338	0.8780	1.73383898	0.87804154
7.0	1.4037	1.6912			1.40364912	1.69120398
10.0	1.3712	1.9067			1.37114859	1.90666356

Table 4. Validation of $f''(0)$, $1/\theta(0)$ for some ε values when $\varphi_{hnf} = \lambda = \delta = 0$ and Pr = 6.2

ε	Waini *et al*. [15]		Present	
	$f''(0)$	$1/\theta(0)$	$f''(0)$	$1/\theta(0)$
5	-10.264749	6.491300	-10.26474930	6.49130024
2	-1.887307	4.203068	-1.88730667	4.20306789
1	0	3.120727	0	3.12072705
0.5	0.713295	2.438276	0.71329495	2.43827646
0.2	1.051130	1.949500	1.05112999	1.94950011
0.1	1.146561	1.767533	1.14656100	1.76753297
0	1.232588	1.573433	1.23258765	1.57343294
-0.1			1.30860209	1.36499970
-0.2			1.37388584	1.13938632
-0.5	1.495670	0.314542	1.49566977	0.31454202
-1	1.328817	-2.359393	1.32881687	-2.35939289

Table 5. Values of $\mathrm{Re}_x^{1/2} C_f$ and $\mathrm{Re}_x^{-1/2} Nu_x$ when $\varphi_1 = 0.01$ and Pr = 6.2

φ_2	K	λ	δ	ε	Al_2O_3-Cu/H_2O	
					$\mathrm{Re}_x^{1/2} C_f$	$\mathrm{Re}_x^{-1/2} Nu_x$
0	0.1	-1	0.1	1	-0.06216211	3.10328071
0.005	0.1	-1	0.1	1	-0.06178147	3.12670063
0.01	0				-0.06221868	3.09889874
	0.1				-0.06141724	3.14890422
	0.2				-0.06065337	3.19837337
	0.1	-1			-0.06141724	3.14890422
		0			0.00000000	3.15650414
		1			0.06079900	3.16396844
		-1	-0.1		-0.05595140	3.34846197
			0		-0.05854949	3.25009566
			0.1	-1	2.29163470	-1.34233968
				0	1.17244042	1.48897470
				1	-0.06141724	3.14890422

Figures 2 and 3 exhibit the differences of $\mathrm{Re}_x^{1/2} C_f$ and $\mathrm{Re}_x^{-1/2} Nu_x$ for several values of K against λ, respectively, when $\varphi_2 = 0.01$, $\delta = 0.1$, and $\varepsilon = 1$. These figures reveal that it is possible for the opposing flow $(\lambda < 0)$ and assisting flow $(\lambda > 0)$ to obtain dual solutions for the stretching $(\varepsilon = 1)$ flow case. The critical solution λ_c (for negative value of λ) and dual solution in the range of λ greater than λ_c exists, but there is no solution is feasible for the range of λ less than λ_c. Beyond this value $\lambda < \lambda_c$, the boundary layer has separated from the surface. It is worth mentioning that the critical point, also known as the bifurcation point, is the joining point between the upper (first) solution and the lower (second) solution. Based on the computations, the bifurcations points for K = 0.0 (flat plate), 0.1, and 0.2 are λ_{c1} = -34.6933, λ_{c2} = -35.7142 and λ_{c3} = -36.7271, respectively. Figure 2 depicts that for both aiding and opposing cases, $\mathrm{Re}_x^{1/2} C_f$ increases with the increment of the curvature parameter K. It is noted that the curvature parameter from the cylinder's outside surface acts like a flat surface when K = 0. As the curvature parameter K approaches 1 $(K \to 1)$, it decreases the viscosity effect because of the surface area with fluid tends to the tangential position. Since the diameter of the cylinder reduces as K rises, the fluid has less contact with the cylinder's surface. Thus, the resistance to the fluid flow decreases, causing an acceleration in the fluid motion. It is also observed that the boundary layer separation for a cylinder is delayed compared to a flat plate. This observation is in accordance with earlier research by Ishak [5]. A similar pattern can also be found in $\mathrm{Re}_x^{-1/2} Nu_x$, as demonstrated in Figure 3. However, for the second solution, $\mathrm{Re}_x^{-1/2} Nu_x$ is unbounded to $\lambda \to 0^+$ and $\lambda \to 0^-$, which is not a physical solution.

Meanwhile, Figures 4 and 5 elucidate the effects of K on $\mathrm{Re}_x^{1/2} C_f$ and $\mathrm{Re}_x^{-1/2} Nu_x$ against stretching/shrinking ε parameter, respectively, for the opposing case $(\lambda < 0)$. Both Figures 4 and 5 show similar trends where the first solution increases with the rise of K, but the second solution shows the opposite outcome. A higher curvature parameter will decrease the viscosity effect of the fluid and thus increase the fluid motion and heat transfer rate. From the numerical computations, the critical value ε_c for K = 0.0, 0.1, and 0.2 are $\varepsilon_c =$ -0.2154, -0.2482 and -0.2796, respectively. From Figures 2 to 5, it can be concluded that $\mathrm{Re}_x^{1/2} C_f$ and $\mathrm{Re}_x^{-1/2} Nu_x$ are higher for a cylinder compared to a flat plate. It can be concluded that these figures (Figures 2-5) allow us to examine the pertinent variables that affect how quickly or slowly boundary layer flow separation from laminar to turbulent.

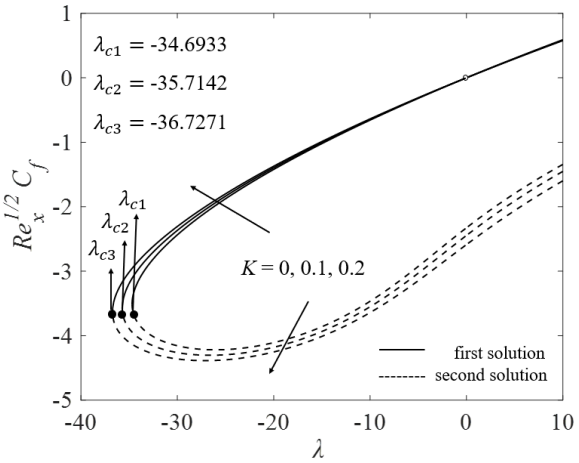

Figure 2. Effects of K on $\mathrm{Re}_x^{1/2} C_f$ against λ when $\varphi_2 = 0.01$, $\delta = 0.1$, and $\varepsilon = 1$ (stretching)

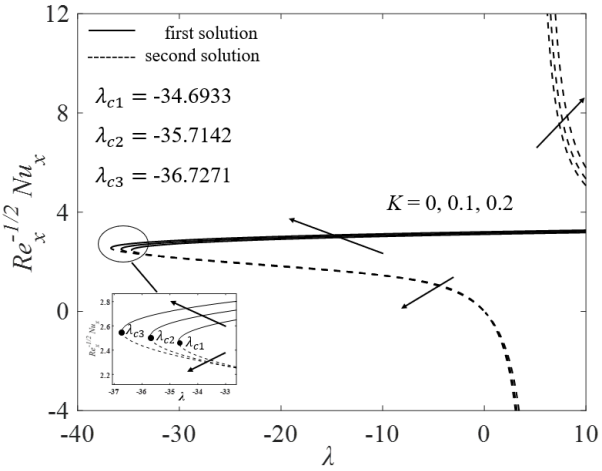

Figure 3. Effects of K on $\mathrm{Re}_x^{-1/2} Nu_x$ against λ when $\varphi_2 = 0.01$, $\delta = 0.1$, and $\varepsilon = 1$ (stretching)

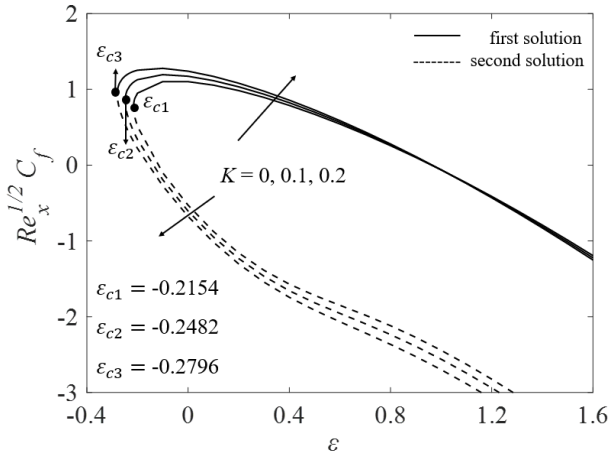

Figure 4. Effects of K on $\mathrm{Re}_x^{1/2} C_f$ against ε when $\varphi_2 = 0.01$, $\delta = 0.1$, and $\lambda = -1$ (opposing)

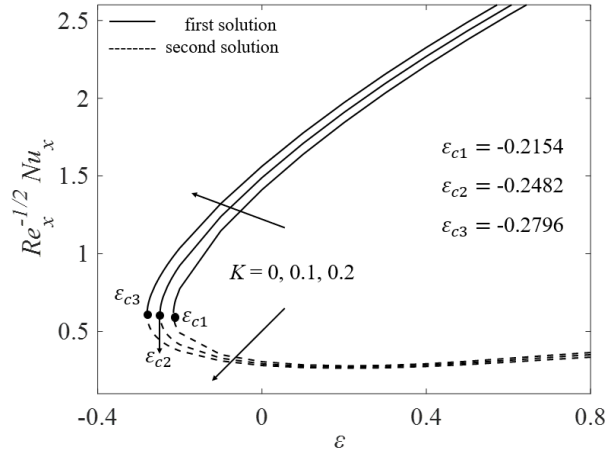

Figure 5. Effects of K on $\mathrm{Re}_x^{-1/2} Nu_x$ against ε when $\varphi_2 = 0.01$, $\delta = 0.1$, and $\lambda = -1$ (opposing)

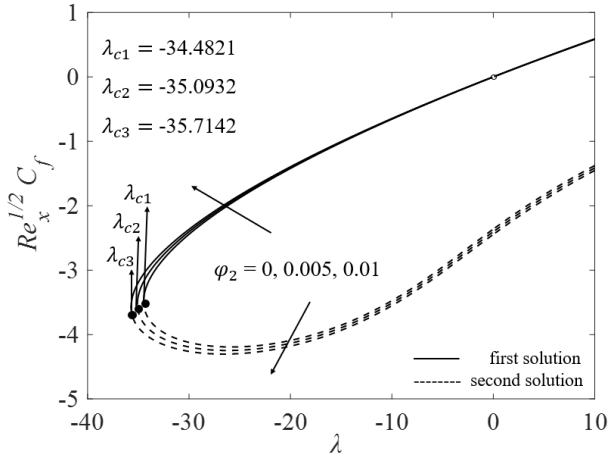

Figure 6. Effects of φ_2 on $\mathrm{Re}_x^{1/2} C_f$ against λ when $K = 0.1$, $\delta = 0.1$, and $\varepsilon = 1$ (stretching)

Further, the influence of the coefficient of skin friction and the local Nusselt number with λ for several values of φ_2, when $K = 0.1$, $\delta = 0.1$, and $\varepsilon = 1$ are portrayed in Figures 6 and 7. The bifurcation values for the Al_2O_3/water nanofluids $(\varphi_1 = 1\%, \varphi_2 = 0\%)$ is $\lambda_{c1} = -34.4821$ and for the Al_2O_3-Cu/water hybrid

nanofluids $(\varphi_1 = 1\%, \varphi_2 = 0.5\%, 1\%)$ are $\lambda_{c2} = -35.0932$ and $\lambda_{c3} = -35.7142$, respectively. Physically, hybrid nanofluids have a greater nanoparticles concentration than nanofluids, which delays the boundary layer separation. From these figures, it is clear that these physical quantities augment with the rising value of φ_2 for the first solution while decreasing for the second solution. Therefore, it is proven that the performance of the fluid's viscosity is enhanced by the higher concentration of nanoparticles. Also, an increment in nanoparticles volume fraction can escalate surface shear stress, thereby increasing the skin friction coefficient $\mathrm{Re}_x^{1/2} C_f$. In addition, Figure 7 presents that $\mathrm{Re}_x^{-1/2} Nu_x$ increases for the higher value the nanoparticles volume fraction φ_2. From the observation, this result suggests that hybrid nanofluids $(\varphi_1 = 1\%, \varphi_2 = 1\%)$ present a better heat transfer rate, as previously mentioned by researchers (see [23,44,45]). This is because hybrid nanofluids have a higher thermal conductivity compared to nanofluids and consequently enhances the heat transfer performance. However, dual behaviors are noticed for the second solution as φ_2 increases where the $\mathrm{Re}_x^{-1/2} Nu_x$ value is unbounded as $\lambda \to 0^+$ and $\lambda \to 0^-$. This finding proves that hybrid nanofluids have better heat transfer enhancement than nanofluids.

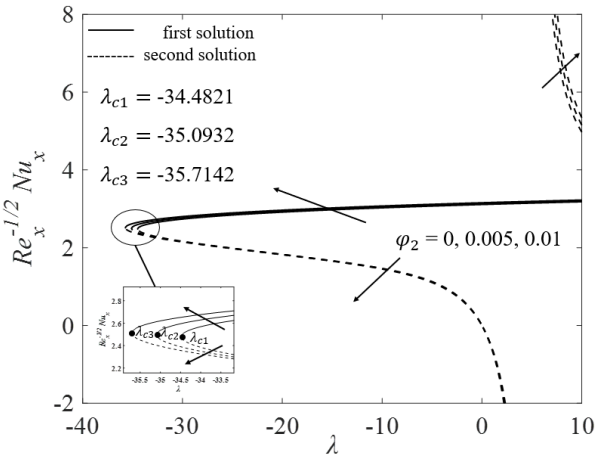

Figure 7. Effects of φ_2 on $\mathrm{Re}_x^{-1/2} Nu_x$ against λ when $K = 0.1$, $\delta = 0.1$, and $\varepsilon = 1$ (stretching)

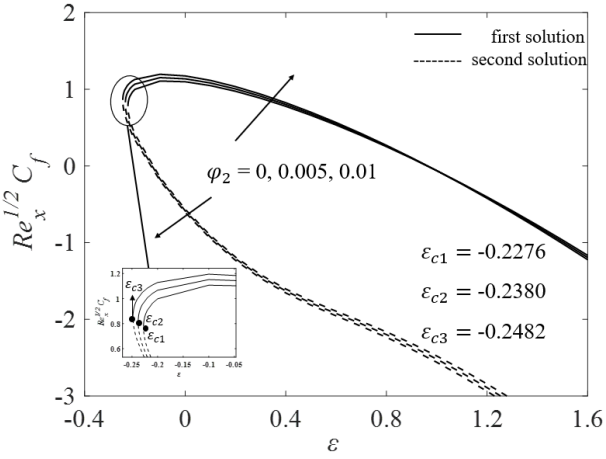

Figure 8. Effects of φ_2 on $\mathrm{Re}_x^{1/2} C_f$ against ε when $K = 0.1$, $\delta = 0.1$, and $\lambda = -1$ (opposing)

Effects of Cu nanoparticles volume fraction φ_2 on the $\mathrm{Re}_x^{1/2} C_f$ and $\mathrm{Re}_x^{-1/2} Nu_x$ against ε are displayed in Figure 8 and 9. It is observed that both figures show similar profile pattern as the φ_2 increases will augment the values of $\mathrm{Re}_x^{1/2} C_f$ and $\mathrm{Re}_x^{-1/2} Nu_x$ for the first solution but declines for the second solution.

Here, the critical value for the Al_2O_3/water nanofluids $(\varphi_1 = 1\%, \varphi_2 = 0\%)$ and for the Al_2O_3-Cu/water hybrid nanofluids $(\varphi_1 = 1\%, \varphi_2 = 0.5\%, 1\%)$ are ε_c = -0.2276, -0.2380 and -0.2482, respectively. It is noted that, between those nanofluids and hybrid nanofluids, the highest critical value is Al_2O_3-Cu/water hybrid nanofluids $(\varphi_1 = 1\%, \varphi_2 = 1\%)$. A similar observation was found in Figures 6 and 7, when φ_2 increases. Hence, this study supports the invention of hybrid nanofluids, which can enhance the heat transfer rate of the working fluid better than the Al_2O_3–water nanofluids. Besides that, hybrid nanoparticles have the capability in increasing the heat transfer rate due to the synergistic effects as mentioned by Waini *et al*. [15].

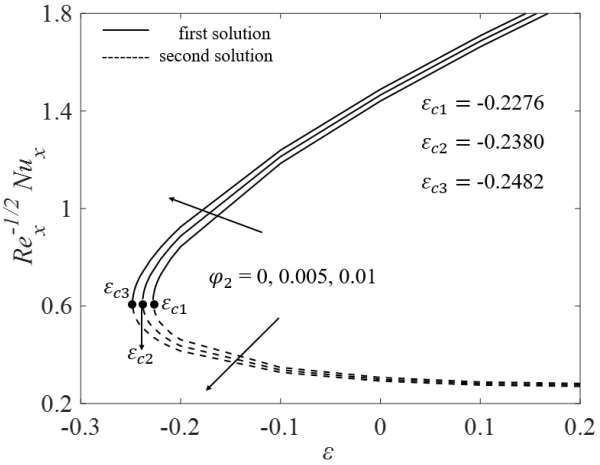

Figure 9. Effects of φ_2 on $\mathrm{Re}_x^{-1/2} Nu_x$ against ε when $K = 0.1$, $\delta = 0.1$, and $\lambda = -1$ (opposing)

Next, Figures 10 and 11 elucidate the influences of heat source $(\delta > 0)$ and heat sink $(\delta < 0)$ parameter on the $\mathrm{Re}_x^{1/2} C_f$ and $\mathrm{Re}_x^{-1/2} Nu_x$ against λ, respectively, for the Al_2O_3-Cu/water hybrid nanofluids. According to Jamaludin *et al*. [32], an increase in the $(\delta < 0)$ indicates an increase in the amount of heat energy supplied by the heat energy reservoir. While, for the decreased $(\delta < 0)$ results in an increase in the amount of heat energy stored in the heat energy reservoir. Figure 10 shows that the increasing value of δ will increase the $\mathrm{Re}_x^{1/2} C_f$ for the assisting flow region $(\lambda > 0)$, while decreasing for the opposing flow region $(\lambda < 0)$. Physically, for the opposing flow $(\lambda < 0)$, buoyancy forces work in the opposite direction of the fluid flow. Thus, this implies that heat sources work by aiding buoyancy, which reduces the fluid flow velocity and minimises the surface shear stress. On the other hand, heat sink $(\delta < 0)$ causes a decrease in buoyancy force and augments the fluid flow velocity which raises the surface shear stress. The variation of the $\mathrm{Re}_x^{-1/2} Nu_x$ against λ with some values of δ is illustrated in Figure 11. It is noticed that $\mathrm{Re}_x^{-1/2} Nu_x$ decreases as δ increases for the range $(-0.1 \le \delta \le 0.1)$. The thickness of the thermal boundary layer is increasing with the presence of a heat source, which causes the declination of the heat flux, which reduces the value of $\mathrm{Re}_x^{-1/2} Nu_x$.

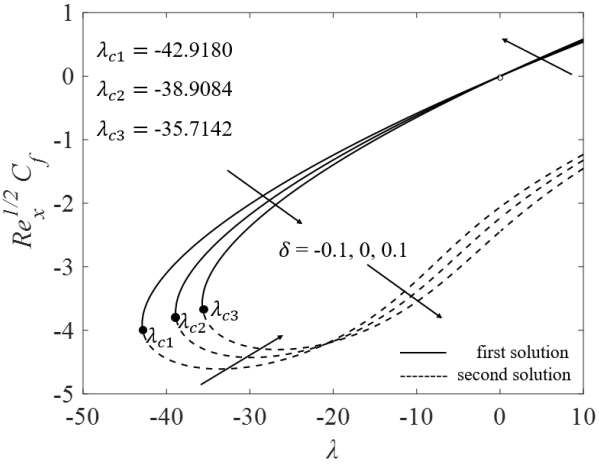

Figure 10. Effects of δ on $\mathrm{Re}_x^{1/2} C_f$ against λ when $K = 0.1$, $\varphi_2 = 0.01$, and $\varepsilon = 1$ (stretching)

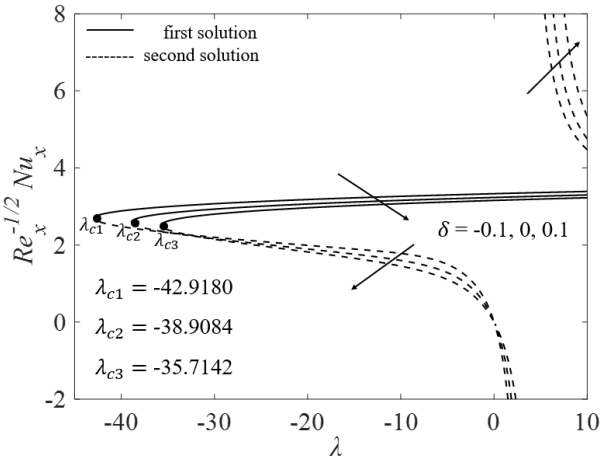

Figure 11. Effects of δ on $\mathrm{Re}_x^{-1/2} Nu_x$ against λ when $K = 0.1$, $\varphi_2 = 0.01$, and $\varepsilon = 1$ (stretching)

Figures 12-17 provide the velocity $f'(\eta)$ and temperature $\theta(\eta)$ profiles for opposing flow $(\lambda = -1)$ and stretching surface $(\varepsilon = 1)$ with $\varphi_2 = 0.01$ and $\delta = 0.1$. Figures 12 and 13 reveal the effects of K on the fluid velocity and temperature, respectively. It is found that as K increases, $f'(\eta)$ decreases for the first solution. When K increases $(0 \le K \le 0.2)$, it indicates that from a flat plate to a cylinder surface, the viscosity effect is decreasing. In addition, the radius of the cylinder is reduced for the higher value of K. A small radius causes less resistance between the fluid and the surface of the cylinder, which consequently accelerates the fluid's motion. Therefore, increase the velocity profile $f'(\eta)$. However, second solution shows that $f'(\eta)$ initially increases then decreases. Figure 13 illustrates the influence of K on the temperature profile $\theta(\eta)$. From the graph, it is shown that the temperature profile is initially decreasing and then increasing as the curvature parameter increases. Kelvin temperature is related to kinetic energy of molecules and is also known as average kinetic energy. When the fluid's velocity increases, so does its kinetic energy, causing the temperature to rise. As a result, the temperature profile decreases near the surface of the cylinder and then increases away from the surface.

Then, the influences of Cu nanoparticles volume fraction φ_2 on both $f'(\eta)$ and $\theta(\eta)$ profiles when $K = 0.1$, $\delta = 0.1$, $\varepsilon = 1$ and $\lambda = -1$ are provided in Figures 14 and 15. It is determined that $f'(\eta)$ and $\theta(\eta)$ increase as the value of φ_2 increases for the first solution but shows the opposite outcome for the

second solution. The results of these figures agree with the illustration in Figures 6 to 9. Figure 14 shows that the velocity profile of Al_2O_3-Cu/water hybrid nanofluids $(\varphi_1 = 1\%, \varphi_2 = 1\%)$ is higher than the Al_2O_3-water nanofluids $(\varphi_1 = 1\%, \varphi_2 = 0\%)$. This scrutiny is consistent with the physical behavior of nanoparticles volume fraction, where the increasing value of φ_2 will augment the concentration of nanoparticles. Hence, decreasing the boundary layer thickness also decelerates the boundary layer separation and thus enhances the fluid flow. Besides that, Figure 15 elucidates a similar trend profile as Figure 14. Similarly, the higher concentration of nanoparticles could exert more energy, lower the surface heat flux, thicken the boundary layer, and thus increase the temperature profile $\theta(\eta)$.

Figures 16 and 17 present $f'(\eta)$ and $\theta(\eta)$ profiles with the changes in heat source/sink parameter δ when $\varphi_2 = 0.01$, $K = 0.1$, $\varepsilon = 1$ and $\lambda = -1$. The positive value of the heat source parameter $(\delta > 0)$ indicates that the heat is generated within the system during flow. While the negative value of the heat sink parameter $(\delta < 0)$ corresponds to heat absorption taking place within the system during the flow. From Figure 16, $f'(\eta)$ decreases with the increase value of δ. The rising of the momentum boundary layer thickness reduces the fluid flow velocity and thus lowers the surface shear stress. This finding is in accordance with that shown in Figure 10, where the increment of δ reduces the skin friction coefficient. Moreover, the temperature profile $\theta(\eta)$ increase with the increasing value of δ. Based on the observations, thermal boundary layer thickness also increases with the increment in δ. The positive increment in the value of δ indicates heat generation, and the heat generated within the system raises the temperature of the fluid flow. Based on these figures, the outcome of this study is in line with the results reported by Jamaludin *et al*. [32].

Subsequently, Figure 18 depicts the smallest eigenvalues γ against the shrinking parameter ε. The sign of γ indicates the stability of the solutions. From the graph, the first solution has a positive γ, which implies that the solution is stable. When $\gamma > 0$, there is an initial decay of disturbance, as mentioned in Equation (18). While the second solution has a negative γ, which indicates that the solution is unstable. When $\gamma < 0$, there is an initial growth of disturbance as time evolves. These observations proved that the upper branch is physically reliable in the long run while the lower branch is not. Besides that, as $\varepsilon \to \varepsilon_c$, $\gamma \to 0$, which is in line with Weidman *et al*. [42], there is transitions occur at the turning point $\varepsilon = \varepsilon_c$ from stable (positive γ) to unstable (negative γ).

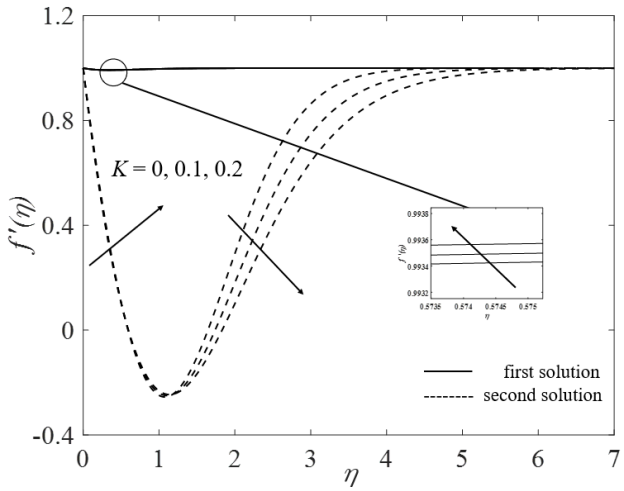

Figure 12. Influence of K on $f'(\eta)$ when $\varphi_2 = 0.01$, $\delta = 0.1$, $\varepsilon = 1$ and $\lambda = -1$

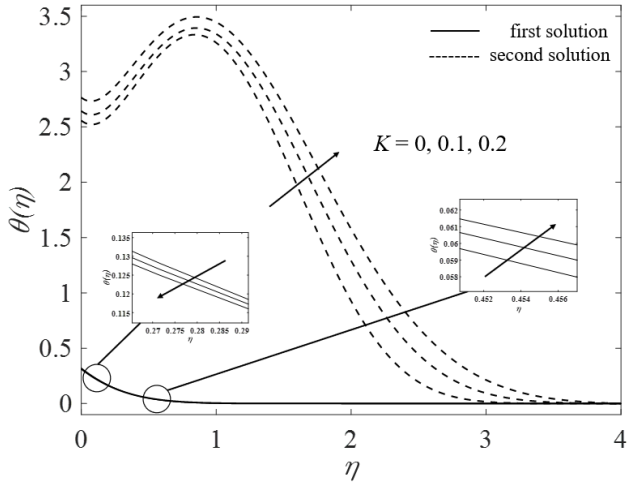

Figure 13. Influence of K on $\theta(\eta)$ when $\varphi_2 = 0.01$, $\delta = 0.1$, $\varepsilon = 1$ and $\lambda = -1$

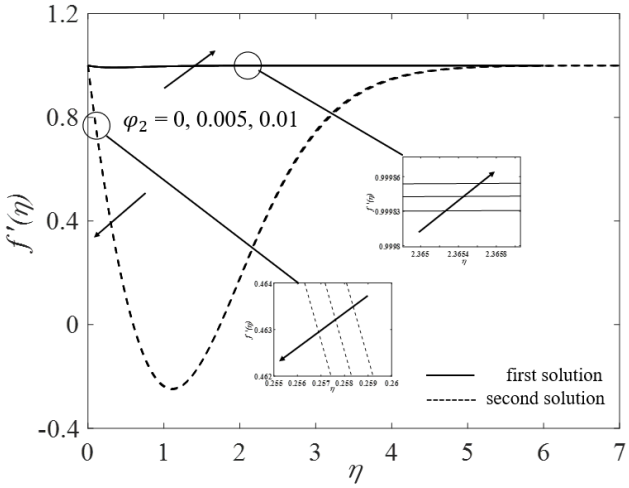

Figure 14. Influence of φ_2 on $f'(\eta)$ when $K = 0.1$, $\delta = 0.1$, $\varepsilon = 1$ and $\lambda = -1$

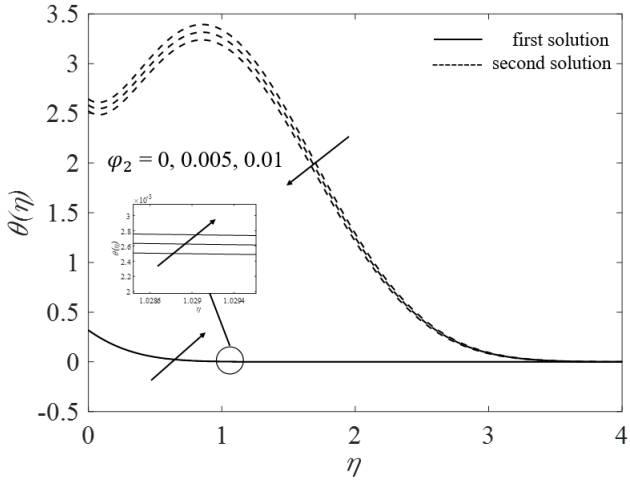

Figure 15. Influence of φ_2 on when $K = 0.1$, $\delta = 0.1$, $\varepsilon = 1$ and $\lambda = -1$

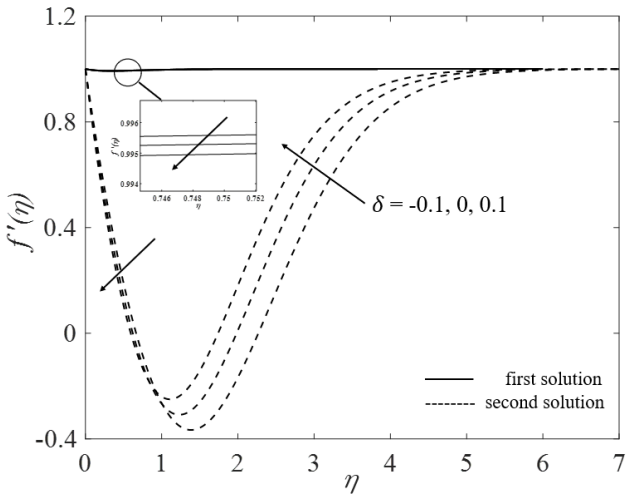

Figure 16. Influence of δ on $f'(\eta)$ when $\varphi_2 = 0.01$, $K = 0.1$, $\varepsilon = 1$ and $\lambda = -1$

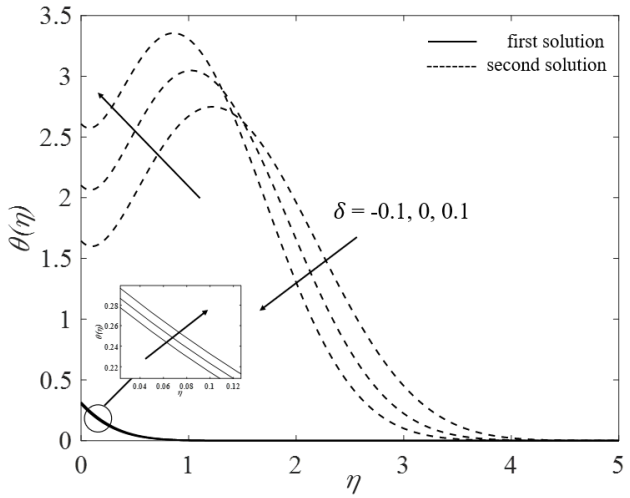

Figure 17. Influence of δ on $\theta(\eta)$ when $\varphi_2 = 0.01$, $K = 0.1$, $\varepsilon = 1$ and $\lambda = -1$

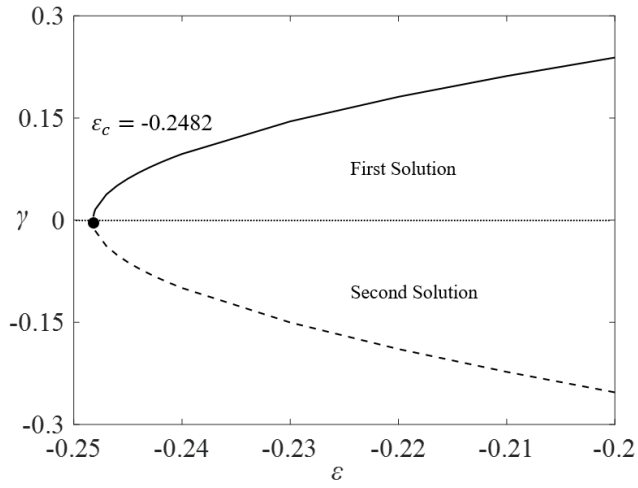

Figure 18. The smallest eigenvalues γ over the shrinking parameter ε

Conclusions

In the present work, a hybrid nanofluids model is developed to study the mixed convection flow over a stretching vertical cylinder with the prescribed surface heat flux and the heat source/sink effects. The present results are in good agreement with those reported in literature. The solutions of the non-dimensionless parameter on the flow, heat and mass transfer characteristics were obtained and graphically illustrated. The findings of the analysis can be summarized as follows:

- Dual solutions can be obtained for both opposing and assisting flow regions and stretching and shrinking surfaces.
- The value of the skin friction and heat transfer on the surface are higher for the cylinder than flat plate.
- In between Al_2O_3/H_2O nanofluids $(\varphi_1 = 1\%, \varphi_2 = 0\%)$ and Al_2O_3-Cu/water hybrid nanofluids $(\varphi_1 = 1\%, \varphi_2 = 0.5\%, 1\%)$, hybrid nanofluids with higher concentration has better performance in heat transfer and velocity of fluid flow.
- An increase of the heat source/sink parameter will decrease the fluid motions and lower the shear stress on the surface.
- Similar trends of $\mathrm{Re}_x^{1/2} C_f$ and $\mathrm{Re}_x^{-1/2} Nu_x$ are observed for the variations of K against the λ and ε cases.
- The outcomes of the stability analysis show that the first solution is stable and reliable, while the second solution is not.

Particularly for researchers studying nanofluids, the model formulation and study results are crucial and useful as guidelines. Future research can examine more parameters, including slip, suction/injection, and magnetic parameters, in greater detail. It's also advised to use different kinds of base fluids and nanoparticles. It is highly recommended that an experimental investigation of this flow problem be carried out for future research, even if this study is theoretical.

Conflicts of Interest

The authors declare that there is no conflict of interest.

Acknowledgment

We would like to thank Universiti Teknologi Malaysia for their helpful feedback and support.

References

[1] Hiemenz, K. (1911). Die Grenzschicht an einem inden gleichförmigen Flüssigkeitsstrom eingetauchten geraden Kreiszylinder. *Dinglers Polytech J.*, *326*, 321-324.
[2] Mahapatra, T.R., & Gupta, A. S. (2002). Heat transfer in stagnation-point flow towards a stretching sheet. *Heat Mass Transf Und Stoffuebertragung*, *38*, 517-5121.
[3] Ishak, A., Nazar, R., & Pop I. (2007). Mixed convection on the stagnation point flow toward a vertical, continuously stretching sheet. *J Heat Transfer*,*129*, 1087-1090.
[4] Wang, C.Y. (2008). Stagnation flow towards a shrinking sheet. *Int J Non Linear Mech*, *43*, 377-82.
[5] Ishak, A. (2009). Mixed convection boundary layer flow over a vertical cylinder with prescribed surface heat flux. *J Phys A Math Theor*, *42*, 195501.
[6] Chen, B., Tian, J. M., & Zhou, Z. F. (2019). The fundamental and application of surface heat flux estimation by inverse method in cryogen spray cooling. In: Suvanjan Bhattacharyya, Mehta R, Ardekani MM, Biswas R, editors. *Inverse Heat Conduct. Heat Exch.*, Rijeka: IntechOpen. 1-19.
[7] Ishak, A., Merkin, J. H., Nazar, R., & Pop, I. (2008). Mixed convection boundary layer flow over a permeable vertical surface with prescribed wall heat flux. *Zeitschrift Fur Angew Math Und Phys*, *59*,100-23.
[8] Ishak, A., Nazar, R., & Pop. I. (2009). MHD flow towards a permeable surface with prescribed wall heat flux. *Chinese Phys Lett*, *26*, 014702.
[9] Ishak, A., Nazar, R., & Pop, I. (2009). MHD convective flow adjacent to a vertical surface with prescribed wall heat flux. *Int Commun Heat Mass Transf*, *36*, 554-557.
[10] Awaludin, I. S., Ahmad, R., & Ishak, A. (2020). On the stability of the flow over a shrinking cylinder with prescribed surface heat flux. *Propuls Power Res*, *9*, 181-187.
[11] Ali, F. M., Nazar, R., & Arifin, N. M. (2010). MHD viscous flow and heat transfer induced by a permeable shrinking sheet with prescribed surface heat flux. *WSEAS Trans Math*, *9*, 365-375.

[12] Aman, F., & Ishak, A. (2010). Hydromagnetic flow and heat transfer adjacent to a stretching vertical sheet with prescribed surface heat flux. *Heat Mass Transf Und Stoffuebertragung*, *46*, 615-620.

[13] Yacob, N. A., & Ishak, A. (2011). MHD flow of a micropolar fluid towards a vertical permeable plate with prescribed surface heat flux. *Chem Eng Res Des*, *89*, 2291-2297.

[14] Waqas, H., Hussain, S., Sharif, H., & Khalid, S. (2017). MHD Forced Convective Flow of Micropolar Fluids Past a Moving Boundary Surface with Prescribed Heat Flux and Radiation. *Br J Math Comput Sci*, *21*, 31270.

[15] Waini, I., Ishak, A., & Pop, I. (2021). Hybrid nanofluid flow on a shrinking cylinder with prescribed surface heat flux. *Int J Numer Methods Heat Fluid Flow*, *31*, 1987-2004.

[16] Daungthongsuk, W., & Wongwises, S. (2007). A critical review of convective heat transfer of nanofluids. *Renew Sustain Energy Rev*, *11*, 797-817.

[17] Ghadimi, A., Saidur, R., & Metselaar, H. S. C. (2011). A review of nanofluid stability properties and characterization in stationary conditions. *Int J Heat Mass Transf*, *54*, 4051-68.

[18] Dhanai, R., Rana, P., & Kumar, L. (2016). MHD mixed convection nanofluid flow and heat transfer over an inclined cylinder due to velocity and thermal slip effects: Buongiorno's model. *Powder Technol*, *288*, 140-50.

[19] Hayat, T., Imtiaz, M., & Alsaedi, A. (2016). Unsteady flow of nanofluid with double stratification and magnetohydrodynamics. *Int J Heat Mass Transf*, *92*, 100-109.

[20] Zaimi, K., Ishak, A., & Pop, I. (2014). Boundary layer flow and heat transfer over a nonlinearly permeable stretching/shrinking sheet in a nanofluid. *Sci Rep*, *4*, 4-11.

[21] Khashi'ie, N. S., Arifin, N. M., Hafidzuddin, E. H., Wahi, N., & Ilias, M. R. (2019). Magnetohydrodynamics (MHD) flow and heat transfer of a doubly stratified nanofluid using Cattaneo-Christov model. *Univers J Mech Eng*, *7*, 206-214.

[22] Khan, M., Hussain, A., Malik, M. Y., Salahuddin, T., & Khan, F. (2017). Boundary layer flow of MHD tangent hyperbolic nanofluid over a stretching sheet: A numerical investigation. *Results Phys*, *7*, 2837-2844.

[23] Suresh, S., Venkitaraj, K. P., Selvakumar, P., & Chandrasekar, M. (2011). Synthesis of Al_2O_3-Cu/water hybrid nanofluids using two step method and its thermo physical properties. *Colloids Surfaces A Physicochem Eng Asp*, *388*, 41-48.

[24] Suresh, S., Venkitaraj, K. P., Selvakumar, P., & Chandrasekar, M. (2012). Effect of Al2O3-Cu/water hybrid nanofluid in heat transfer. *Exp Therm Fluid Sci*. *38*, 54-60.

[25] Takabi, B., & Salehi, S. (2014). Augmentation of the heat transfer performance of a sinusoidal corrugated enclosure by employing hybrid nanofluid. *Adv Mech Eng*, *2014*, 147059.

[26] Devi, S. S. U., Devi, S. P. A. (2016). Numerical investigation of three-dimensional hybrid Cu-Al_2O_3/water nanofluid flow over a stretching sheet with effecting Lorentz force subject to Newtonian heating. *Can J Phys*., *94*(5), 490-496.

[27] Devi, S. S. U., & Devi, S. P. A. (2017). Heat transfer enhancement of Cu−Al_2O_3/water hybrid nanofluid flow over a stretching sheet. *J Niger Math Soc*., *36*(2), 419-433.

[28] Rostami, M. N., Dinarvand, S., & Pop, I. (2018). Dual solutions for mixed convective stagnation-point flow of an aqueous silica–alumina hybrid nanofluid. *Chinese J Phys.*, *56*(5), 2465-2478.

[29] Subhani, M., & Nadeem, S. (2019). Numerical analysis of micropolar hybrid nanofluid. *Appl Nanosci*, *9*(4), 447-459.

[30] Zainal, N. A., Nazar, R., Naganthran, K., & Pop, I. (2020). Unsteady three-dimensional MHD non-axisymmetric homann stagnation point flow of a hybrid nanofluid with stability analysis. *Mathematics*, *8*(5), 784.

[31] Sohut, F. H., Ishak, A., & Soid, S. K. (2023). MHD stagnation point of Blasius flow for micropolar hybrid nanofluid toward a vertical surface with stability analysis. *Symmetry (Basel)*,*15*(4), 920.

[32] Jamaludin, A., Naganthran, K., Nazar, R., & Pop, I. (2020). MHD mixed convection stagnation-point flow of Cu-Al2O3/water hybrid nanofluid over a permeable stretching/shrinking surface with heat source/sink. *Eur J Mech B/Fluids*, *84*, 71-80.

[33] Gorla, R. S. R., Siddiqa, S., Mansour, M. A., Rashad, A. M., & Salah, T. (2017). Heat source/sink effects on a hybrid nanofluid-filled porous cavity. *J Thermophys Heat Transf*, *31*, 847-857.

[34] Armaghani, T., Sadeghi, M. S., Rashad, A. M., Mansour, M. A., Chamkha, A. J., Dogonchi, A.S, *et al*. (2021). MHD mixed convection of localized heat source/sink in an Al_2O_3-Cu/water hybrid nanofluid in L-shaped cavity. *Alexandria Eng J*, *60*, 2947-2962.

[35] Yaseen, M., Kumar, M., & Rawat, S. K. (2021). Assisting and opposing flow of a MHD hybrid nanofluid flow past a permeable moving surface with heat source/sink and thermal radiation. *Partial Differ Equations Appl Math*, *4*,100168.

[36] Farooq, U., Tahir, M., Waqas, H., Muhammad, T., Alshehri, A., & Imran, M. (2022). Investigation of 3D flow of magnetized hybrid nanofluid with heat source/sink over a stretching sheet. *Sci Rep*, *12*, 12254.

[37] Sadighi, S., Afshar, H., Jabbari, M. & Ashtiani, H. A. D. (2023). Heat and mass transfer for MHD nanofluid flow on a porous stretching sheet with prescribed boundary conditions. *Case Stud Therm Eng.*, *49*, 103345.

[38] Oztop, H. F., & Abu-Nada, E. (2008). Numerical study of natural convection in partially heated rectangular enclosures filled with nanofluids. *Int J Heat Fluid Flow*, *29*(5), 1326-1336.

[39] Waini, I., Ishak, A., & Pop, I. (2019). Hybrid nanofluid flow and heat transfer past a vertical thin needle with prescribed surface heat flux. *Int J Numer Methods Heat Fluid Flow*, *29*(12), 4875-4894.

[40] Khashi'ie, N. S., Arifin, N. M., & Pop, I. (2020). Mixed convective stagnation point flow towards a vertical riga plate in hybrid Cu-Al_2O_3/water nanofluid. *Mathematics*, *8*(6), 912.

[41] Merkin, J. H. (1986).On dual solutions occurring in mixed convection in a porous medium. *J Eng Math*, *20*, 171-179.

[42] Weidman, P. D., Kubitschek, D. G., & Davis, A. M. J. (2006). The effect of transpiration on self-similar boundary layer flow over moving surfaces. *Int J Eng Sci*, *44*, 730-737.

[43] Harris, S. D., Ingham, D. B., & Pop, I. (2009). Mixed convection boundary-layer flow near the stagnation point on a vertical surface in a porous medium: Brinkman model with slip. *Transp Porous Media*, *77*(2), 267-85.

[44] Devi, S. S. U., & Devi, S. P. A. (2017). Heat transfer enhancement of Cu−Al_2O_3/water hybrid nanofluid flow

over a stretching sheet. *J Niger Math Soc*, *36*(2), 419-433.
[45] Khashi'ie, N. S., Arifin, N. M., Merkin, J. H., Yahaya, R. I., & Pop, I. (2021). Mixed convective stagnation point flow of a hybrid nanofluid toward a vertical cylinder. *Int J Numer Methods Heat Fluid Flow*, *31*(12), 3689-3710.